Supporting Information

Shi et al. 10.1073/pnas.1708944114

SI Text

This *SI Text* is divided into four sections. *Light Propagation in Single-Segment Nonlinear Fiber* is devoted to analyzing the light propagation in the fiber with a Kerr medium. In *Steady-state solutions and fluctuations in fibers*, we establish the nonlinear motion equations to describe the light propagation in the horizontal and vertical fibers. By solving the motion equations, we investigate the properties of steady states and Bogoliubov fluctuations. To get insight into the steady-state stability of the whole network, in *Nonlinear Fabry–Perot cavity*, we analyze the stability of steady states in a single nonlinear Fabry–Perot cavity as a paradigmatic example.

Using the S matrices at each node (*Steady-State Solutions* in the main text) and in fibers (*Light Propagation in Single-Segment Nonlinear Fiber*), in *Scattering Equations on Different Geometries* we derive a nonlinear scattering equation in the network with different geometries, which determines the steady-state properties.

In *Robustness of Broadband Setups*, we show that broadband models are able to be immune to losses and perturbations. To illustrate the advantages of broadband models compared with the narrow ones, we build a new setup, in which the width of the topological bandgap can be tuned. The edge currents in the networks with the broad and narrow bands are shown to reveal the robustness of edge modes in the broadband network, where the intrinsic losses are the same in the two networks. In *Propagation Matrices of Bogoliubov Excitations*, the matrices used in the Bogoliubov fluctuation analysis are defined.

Light Propagation in Single-Segment Nonlinear Fiber. This section is divided into two subsections. In *Steady-state solutions and fluctuations in fibers*, the light propagation in a fiber with the nonlinear Kerr medium is analyzed. In *Nonlinear Fabry–Perot cavity*, a simple nonlinear system, i.e., the Fabry–Perot cavity, is analyzed, where the stability of steady states is investigated.

Steady-state solutions and fluctuations in fibers. The formal solutions of Eqs. **4** and **5** in *Light Propagation in Fibers* of the main text are

$$\begin{aligned}\phi_{r,nm}(x,t)&=[a_{r,nm}+\delta\phi_{r,nm}(x,t)]e^{ik_r(x-L)}e^{-i\omega t},\\ \phi_{l,nm-1}(x,t)&=[\tilde{a}_{l,nm-1}+\delta\phi_{l,nm-1}(x,t)]e^{-ik_l x}e^{-i\omega t},\end{aligned}\qquad\textbf{[S1]}$$

where $\delta\phi_{r,nm}$ and $\delta\phi_{l,nm-1}$ are the fluctuation fields around the steady state. For the closed network, the characteristic frequency $\omega=\mathcal{E}$ is the eigenfrequency, and $\omega=\omega_{\rm d}$ is the frequency of the driving field applied to the open network. The steady-state solution gives rise to the relation **6** in the main text.

The fluctuation field $\delta\Psi=(\delta\phi_{r,nm},\delta\phi_{l,nm-1},\delta\phi^*_{r,nm},\delta\phi^*_{l,nm-1})^T$ obeys the linearized motion equation

$$i\partial_t\delta\Psi+\Sigma\partial_x\delta\Psi=\mathbf{M}_H\delta\Psi,\qquad\textbf{[S2]}$$

where the matrices are

$$\Sigma=i\begin{pmatrix}1&0&0&0\\0&-1&0&0\\0&0&1&0\\0&0&0&-1\end{pmatrix},\qquad\textbf{[S3]}$$

and

$$\mathbf{M}_H=\chi\begin{pmatrix}|a_{r,nm}|^2&2\tilde{a}^*_{l,nm-1}a_{r,nm}&a^2_{r,nm}&2a_{r,nm}\tilde{a}_{l,nm-1}\\2a^*_{r,nm}\tilde{a}_{l,nm-1}&|\tilde{a}_{l,nm-1}|^2&2a_{r,nm}\tilde{a}_{l,nm-1}&\tilde{a}^2_{l,nm-1}\\-a^{*2}_{r,nm}&-2a^*_{r,nm}\tilde{a}^*_{l,nm-1}&-|a_{r,nm}|^2&-2a^*_{r,nm}\tilde{a}_{l,nm-1}\\-2a^*_{r,nm}\tilde{a}^*_{l,nm-1}&-\tilde{a}^{*2}_{l,nm-1}&-2\tilde{a}^*_{l,nm-1}a_{r,nm}&-|\tilde{a}_{l,nm-1}|^2\end{pmatrix}.\qquad\textbf{[S4]}$$

The Bogoliubov mode $\delta\Psi=\delta\psi e^{-i\omega_{\rm f}t}$ with the fluctuation frequency $\omega_{\rm f}$ around ω obeys the equation

$$\omega_{\rm f}\delta\psi+\Sigma\partial_x\delta\psi=\mathbf{M}_H\delta\psi,\qquad\textbf{[S5]}$$

where the time-independent field

$$\delta\psi=(\delta\psi_{r,nm},\delta\psi_{l,nm-1},\delta\psi^*_{r,nm},\delta\psi^*_{l,nm-1})^T.\qquad\textbf{[S6]}$$

The formal solution of Eq. **S5** leads to the relation

$$e^{\Sigma(\omega_{\rm f}-\mathbf{M}_H)L}\begin{pmatrix}e^{-in\sigma\theta_0}\delta b_{r,nm}\\e^{-in\sigma\theta_0}\delta a_{l,nm-1}\\e^{in\sigma\theta_0}\delta b^*_{r,nm}\\e^{in\sigma\theta_0}\delta a^*_{l,nm-1}\end{pmatrix}=\begin{pmatrix}\delta a_{r,nm}\\\delta b_{l,nm-1}\\\delta a^*_{r,nm}\\\delta b^*_{l,nm-1}\end{pmatrix}\qquad\textbf{[S7]}$$

of the input and output fluctuation fields

$$\delta a_{r,nm}=\delta\psi_{r,nm}(L),\delta a_{l,nm-1}=e^{in\sigma\theta_0}\delta\psi_{l,nm-1}(0),\qquad\textbf{[S8]}$$

and

$$\delta b_{r,nm}=e^{in\sigma\theta_0}\delta\psi_{r,nm}(0),\delta b_{l,nm-1}=\delta\psi_{l,nm-1}(L),\qquad\textbf{[S9]}$$

around the steady-state amplitudes $a_{r,nm}$ ($\delta a_{l,nm-1}$) and $b_{r,nm}$ ($b_{l,nm-1}$).

The same analysis is applied to light propagation in the vertical fiber connecting nodes (n, m) and $(n+1, m)$, which leads to Eq. **9** in *Light Propagation in Fibers* in the main text. By linearizing the motion equation in the vertical fiber around the steady-state solution $a_{u,nm}$ $(a_{d,n+1m})$ and $b_{u,nm}$ $(b_{d,n+1m})$, we establish the relation

$$e^{\Sigma(\omega_{\rm f}-\mathbf{M}_V)L}\begin{pmatrix}\delta b_{u,nm}\\ \delta a_{d,n+1m}\\ \delta b^*_{u,nm}\\ \delta a^*_{d,n+1m}\end{pmatrix}=\begin{pmatrix}\delta a_{u,nm}\\ \delta b_{d,n+1m}\\ \delta a^*_{u,nm}\\ \delta b^*_{d,n+1m}\end{pmatrix} \quad \textbf{[S10]}$$

of the input and output fluctuation fields $\delta a_{u,nm}$ $(\delta a_{d,n+1m})$ and $\delta b_{u,nm}$ $(\delta b_{d,n+1m})$, where

$$\mathbf{M}_V=\chi\begin{pmatrix}|a_{u,nm}|^2 & 2a^*_{d,n+1m}a_{u,nm} & a^2_{u,nm} & 2a_{u,nm}a_{d,n+1m}\\ 2a^*_{u,nm}a_{d,n+1m} & |a_{d,n+1m}|^2 & 2a_{u,nm}a_{d,n+1m} & a^2_{d,n+1m}\\ -a^{*2}_{u,nm} & -2a^*_{u,nm}a^*_{d,n+1m} & -|a_{u,nm}|^2 & -2a^*_{u,nm}a_{d,n+1m}\\ -2a^*_{u,nm}a^*_{d,n+1m} & -a^{*2}_{d,n+1m} & -2a^*_{d,n+1m}a_{u,nm} & -|a_{d,n+1m}|^2\end{pmatrix}. \quad \textbf{[S11]}$$

Nonlinear Fabry–Perot cavity. Before studying the steady-state properties and the stability of the light in the whole network, we use a paradigmatic example, i.e., the single Fabry–Perot cavity with nonlinear Kerr medium (47), to show the stability analysis of steady states. Our goal is to understand better the stability analysis for more complex 2D arrays of nonlinear fibers and beam splitters.

As shown in Fig. S1, the cavity with a perfect right end mirror is driven by the light with frequency $\omega_{\rm d}$ through a partially transmissive mirror at the left end. In the cavity, the phase plate is placed next to the transmissive mirror. In propagation from left to right, the light acquires the phase factor $e^{-i\theta_0}$. Here, $\theta_0 \neq 0$ $(\theta_0 = 0)$ corresponds to the single horizontal (vertical) fiber in the network.

The relations

$$e^{-i\theta_0}b_r = e^{-ik_r L}a_r,\ e^{i\theta_0}b_l = e^{-ik_l L}a_l \quad \textbf{[S12]}$$

of input a_r (a_l) and output amplitude b_r (b_l) follow from Eq. **8** in the main text, where L is the cavity length, and

$$\begin{aligned}k_r &= \omega_{\rm d}-\chi(|a_r|^2+2|a_l|^2),\\ k_l &= \omega_{\rm d}-\chi(|a_l|^2+2|a_r|^2).\end{aligned} \quad \textbf{[S13]}$$

At the end mirrors, the boundary conditions are $a_r = b_l$, and

$$\begin{pmatrix}b_r\\ A^{(0)}_{\rm out}\end{pmatrix}=\begin{pmatrix}t_{\rm BM} & ir_{\rm BM}\\ ir_{\rm BM} & t_{\rm BM}\end{pmatrix}\begin{pmatrix}A^{(0)}_{\rm in}\\ a_l\end{pmatrix}, \quad \textbf{[S14]}$$

where $t_{\rm BM}$ $(r_{\rm BM})$ is the real transmission (reflection) coefficient of the left end mirror, and $A^{(0)}_{\rm in}$ $(A^{(0)}_{\rm out})$ is the input (output) amplitude of the cavity.

By eliminating the output amplitude b_r (b_l) in Eqs. **S12** and **S14**, we obtain the nonlinear equation

$$a_r = \frac{t_{\rm BM}A^{(0)}_{\rm in}e^{-i\theta_0}}{e^{-ikL}-ir_{\rm BM}e^{ikL}} \quad \textbf{[S15]}$$

that determines the amplitude $a_r = |a_r|\,e^{i\theta_r}$, where $k_r = k_l \equiv k = \omega_{\rm d} - 3\chi|a_r|^2$, and the output amplitude

$$A^{(0)}_{\rm out} = ir_{\rm BM}A^{(0)}_{\rm in}+t_{\rm BM}a_l = \frac{e^{ikL}+ir_{\rm BM}e^{-ikL}}{e^{-ikL}-ir_{\rm BM}e^{ikL}}A^{(0)}_{\rm in} \quad \textbf{[S16]}$$

of the cavity is determined by the relation $a_l = e^{i\theta_0}e^{ikL}a_r$. In the good cavity limit $t_{\rm BM}\to 0$, Eq. **S15** determines the intensity-dependent frequency

$$\mathcal{E}_n = \frac{n\pi}{L}-\frac{\pi}{4L}+3\chi|a_r|^2 \quad \textbf{[S17]}$$

of the closed cavity, where n is an integer.

For different driving frequency $\omega_{\rm d}$, the relation

$$x = \frac{y}{1-r^2_{\rm BM}}[1+r^2_{\rm BM}+2r_{\rm BM}\sin(2\omega_{\rm d}L-6y)] \quad \textbf{[S18]}$$

of $y=\chi|a_r|^2$ and the input intensity $x=\chi\left|A^{(0)}_{\rm in}\right|^2$ is shown in Fig. S2 *A* and *B*, where $L=1$ is taken as a unit and $r_{\rm BM}=0.85, 0.9, 0.95$. When the driving frequency $\omega_{\rm d}$ is resonant with the intrinsic frequency $\mathcal{E}_n$ of the closed cavity, the output field $A^{(0)}_{\rm out}=-iA^{(0)}_{\rm in}$.

Fig. S2 *A* and *B* shows that for a given $\omega_{\rm d}$, the driving field with a fixed intensity $\left|A^{(0)}_{\rm in}\right|^2$ can generate multiple intracavity intensities. To analyze the stability of these multiple steady states, we investigate the energy spectrum of Bogoliubov fluctuations. It follows from Eq. **S7** that the fluctuation fields satisfy

$$e^{\Sigma(\omega_{\rm f}-U^\dagger_{\rm s}\mathbf{M}_{\rm s}U_{\rm s})L}\begin{pmatrix}e^{-i\theta_0}\delta b_r\\ e^{-i\theta_0}\delta a_l\\ e^{i\theta_0}\delta b^*_r\\ e^{i\theta_0}\delta a^*_l\end{pmatrix}=\begin{pmatrix}\delta a_r\\ \delta b_l\\ \delta a^*_r\\ \delta b^*_l\end{pmatrix}, \quad \textbf{[S19]}$$

where the matrix

$$\mathbf{M}_\mathrm{s} = \chi|a_r|^2 \begin{pmatrix} 1 & 2e^{-ikL} & 1 & 2e^{ikL} \\ 2e^{ikL} & 1 & 2e^{ikL} & e^{2ikL} \\ -1 & -2e^{-ikL} & -1 & -2e^{ikL} \\ -2e^{-ikL} & -e^{-2ikL} & -2e^{-ikL} & -1 \end{pmatrix} \quad \text{[S20]}$$

for the single fiber, and the unitary matrix $U_\mathrm{s} = I_2 \oplus e^{2i\theta_r} I_2$ is determined by the 2D identity matrix I_2.

The fluctuation Eq. **S19** leads to the relation $\delta\mathbf{B} = \tilde{U}_\theta U_b^{-1} U_a U_\theta \delta\mathbf{A}$ of $\delta\mathbf{B} = (\delta b_r, \delta b_l, \delta b_r^*, \delta b_l^*)^T$ and $\delta\mathbf{A} = (\delta a_r, \delta a_l, \delta a_r^*, \delta a_l^*)^T$, where the matrices

$$U_a = \begin{pmatrix} 1 & -P_{\mathrm{s},12} & 0 & -P_{\mathrm{s},14} \\ 0 & P_{\mathrm{s},22} & 0 & P_{\mathrm{s},24} \\ 0 & -P_{\mathrm{s},32} & 1 & -P_{\mathrm{s},34} \\ 0 & P_{\mathrm{s},42} & 0 & P_{\mathrm{s},44} \end{pmatrix},$$

$$U_b = \begin{pmatrix} P_{\mathrm{s},11} & 0 & P_{\mathrm{s},13} & 0 \\ -P_{\mathrm{s},21} & 1 & -P_{\mathrm{s},23} & 0 \\ P_{\mathrm{s},31} & 0 & P_{\mathrm{s},33} & 0 \\ -P_{\mathrm{s},41} & 0 & -P_{\mathrm{s},43} & 1 \end{pmatrix} \quad \text{[S21]}$$

are determined by the propagating matrix $P_\mathrm{s} = e^{\Sigma(\omega_\mathrm{f} - U_\mathrm{s}^\dagger \mathbf{M}_\mathrm{s} U_\mathrm{s})L}$, and the diagonal matrices

$$U_\theta = \begin{pmatrix} 1 & 0 & 0 & 0 \\ 0 & e^{-i\theta_0} & 0 & 0 \\ 0 & 0 & 1 & 0 \\ 0 & 0 & 0 & e^{i\theta_0} \end{pmatrix}, \tilde{U}_\theta = \begin{pmatrix} e^{i\theta_0} & 0 & 0 & 0 \\ 0 & 1 & 0 & 0 \\ 0 & 0 & e^{-i\theta_0} & 0 \\ 0 & 0 & 0 & 1 \end{pmatrix}. \quad \text{[S22]}$$

On the other hand, the boundary conditions at the end mirrors are $\delta a_r = \delta b_l e^{-ikL}$ and

$$\begin{pmatrix} \delta b_r e^{-ikL} \\ \delta A_\mathrm{out} \end{pmatrix} = \begin{pmatrix} t_\mathrm{BM} & ir_\mathrm{BM} \\ ir_\mathrm{BM} & t_\mathrm{BM} \end{pmatrix} \begin{pmatrix} \delta A_\mathrm{in} \\ \delta a_l \end{pmatrix}. \quad \text{[S23]}$$

By eliminating the fluctuation field δB, we obtain the scattering equation

$$(\tilde{U}_\theta U_b^{-1} U_a U_\theta - U_k R_\mathrm{BM})\delta\mathbf{A} = t_\mathrm{BM} U_k \delta\mathbf{A}_d \quad \text{[S24]}$$

with the driving term $\delta\mathbf{A}_d = (\delta A_\mathrm{in}, 0, \delta A_\mathrm{in}^*, 0)^T$, where the matrices $U_k = e^{ikL} I_2 \oplus e^{-ikL} I_2$ and

$$R_\mathrm{BM} = \begin{pmatrix} 0 & ir_\mathrm{BM} & 0 & 0 \\ 1 & 0 & 0 & 0 \\ 0 & 0 & 0 & -ir_\mathrm{BM} \\ 0 & 0 & 1 & 0 \end{pmatrix}. \quad \text{[S25]}$$

The zeros $D(\mathcal{E}_\mathrm{f}) = 0$ of the determinant

$$D(\omega_\mathrm{f}) = \det(\tilde{U}_\theta U_b^{-1} U_a U_\theta - U_k R_\mathrm{BM}) \quad \text{[S26]}$$

determine the stability of the steady-state solution, where the steady state is stable if all $\mathrm{Im}\mathcal{E}_\mathrm{f} < 0$.

For the good cavity limit $t_\mathrm{BM} \to 0$, the momentum $kL = n\pi - \pi/4$, and the eigenfrequency of Bogoliubov fluctuations is $\mathcal{E}_\mathrm{f} = n_\mathrm{f}\pi$, where n_f is an integer. For the open cavity, the condition $D(\mathcal{E}_\mathrm{f}) = 0$ leads to the two transcendental equations

$$\begin{aligned} \mathrm{Re}D(x_1 + ix_2) &= 0, \\ \mathrm{Im}D(x_1 + ix_2) &= 0, \end{aligned} \quad \text{[S27]}$$

for x_1 =Re$\mathcal{E}_\mathrm{f}$ and x_2 =Im$\mathcal{E}_\mathrm{f}$. In Fig. S2 *C* and *D*, we show the two curves given by Eq. **S27** for different driving intensities $\chi\left|A_\mathrm{in}^{(0)}\right|^2$, where the intersection of two curves determines the solution x_1 and x_2. As shown in Fig. S2*D*, the positive coordinates $x_2 > 0$ at points of intersection imply an unstable steady state. In Fig. S2 *A* and *B*, the stable regimes are marked by the black circles, where these stable solutions are in the positive slope regimes of $\chi|a_r|^2$ vs. $\chi\left|A_\mathrm{in}^{(0)}\right|^2$ curves.

Scattering Equations on Different Geometries. In this section, we use Eqs. **8** and **9** in the main text to derive the scattering equation for the steady-state amplitudes $a_{r,u,l,d}$ in the nonlinear network. Here, in terms of different boundary conditions, we analyze the scattering equations describing the closed and open networks on three kinds of geometries.

Combining Eqs. **8** and **9** and the node S-matrix **3** in the main text, we obtain the scattering equation

$$S_0 \begin{pmatrix} a_{r,nm} \\ a_{u,nm} \\ a_{l,nm} \\ a_{d,nm} \end{pmatrix} = e^{-i\omega L} e^{i\chi\mathcal{N}_{nm}L} \begin{pmatrix} a_{r,nm+1} \\ a_{u,n-1m} \\ a_{l,nm-1} \\ a_{d,n+1m} \end{pmatrix} \quad \text{[S28]}$$

for the input amplitudes at the bulk nodes, where the phase shift induced by the Kerr nonlinearity is depicted by the intensity matrix

$$\mathcal{N}_{nm} = \begin{pmatrix} |a_{r,nm+1}|^2 + 2|a_{l,nm}|^2 & 0 & 0 & 0 \\ 0 & |a_{u,n-1m}|^2 + 2|a_{d,nm}|^2 & 0 & 0 \\ 0 & 0 & |a_{l,nm-1}|^2 + 2|a_{r,nm}|^2 & 0 \\ 0 & 0 & 0 & |a_{d,n+1m}|^2 + 2|a_{u,nm}|^2 \end{pmatrix}. \quad \text{[S29]}$$

Without the Kerr nonlinearity, i.e., $\chi = 0$, the scattering Eq. **S28** becomes Eq. **17** in the main text for the linear network.

Closed network. The boundary conditions for networks in the torus, cylinder, and open plane are given by Eqs. **11–13** in *Full Networks* in the main text. For the networks in the torus and cylinder, due to the translational symmetry, the solution has the form **19** in the main text, and the scattering Eq. **S28** becomes

$$S_0(k_x)\begin{pmatrix} a_{r,n} \\ a_{u,n} \\ a_{l,n} \\ a_{d,n} \end{pmatrix} = e^{-i\mathcal{E}L} e^{i\frac{\chi}{N_x}\mathcal{N}_n L}\begin{pmatrix} a_{r,n} \\ a_{u,n-1} \\ a_{l,n} \\ a_{d,n+1} \end{pmatrix}, \qquad \textbf{[S30]}$$

where the intensity matrix along the row of the network is

$$\mathcal{N}_n = \begin{pmatrix} |a_{r,n}|^2 + 2|a_{l,n}|^2 & 0 & 0 & 0 \\ 0 & |a_{u,n-1}|^2 + 2|a_{d,n}|^2 & 0 & 0 \\ 0 & 0 & |a_{l,n}|^2 + 2|a_{r,n}|^2 & 0 \\ 0 & 0 & 0 & |a_{d,n+1}|^2 + 2|a_{u,n}|^2 \end{pmatrix}. \qquad \textbf{[S31]}$$

By taking into account the boundary conditions **11** and **12** in the main text, the scattering equation for the entire closed network in the torus and cylinder can be written as

$$S_0(k_x)\mathbf{a} = e^{-i\mathcal{E}L} e^{i\frac{\chi}{N_x}\mathcal{N}_n L}\mathbf{a} \qquad \textbf{[S32]}$$

in the basis $\mathbf{a} = (a_{r,n}, a_{u,n}, a_{l,n}; a_{d,n})^T$.

Similarly, by the boundary condition **13** in the main text, the scattering equation for the closed networks in the plane reads

$$S_0\mathbf{a} = e^{-i\mathcal{E}L} e^{i\chi\mathcal{N}L}\mathbf{a} \qquad \textbf{[S33]}$$

in the basis $\mathbf{a} = (a_{r,nm}, a_{u,nm}, a_{l,nm}, a_{d,nm})^T$.

In the main text, we numerically solve Eqs. **32** and **33** for the linear closed network, i.e., $\chi = 0$, and show the spectra $\mathcal{E}$ of the network with different geometries. For the closed nonlinear network, i.e., $\chi \neq 0$, the solutions are unstable in general. To generate and stabilize the state of light with Kerr nonlinearities, we drive the network through the top boundary mirrors of the cylindrical open network.

Open network. For the open network in the cylinder shown in Fig. 2 *A* and *C* of the main text, the nonlinear scattering equation for the amplitude $\mathbf{a} = (a_{r,n}, a_{u,n}, a_{l,n}; a_{d,n})^T$ reads

$$R_{\mathrm{BM}} S_0(k_x)\mathbf{a} = e^{-i\omega_{\mathrm{d}}L} e^{i\frac{\chi}{N_x}\mathcal{N}_n L}\mathbf{a} - t_{\mathrm{BM}} e^{-i\omega_{\mathrm{d}}L/2}\mathbf{A}_{\mathrm{in}}^{(0)}, \qquad \textbf{[S34]}$$

where R_{BM} is obtained by replacing the diagonal matrix element $I_{3N_y+1,3N_y+1}$ of the $4N_y$-dimensional identity matrix I by ir_{BM}, and $\mathbf{A}_{\mathrm{in}}^{(0)} = A_{\mathrm{in}}^{(0)}(\mathbf{0};\mathbf{0};\mathbf{0};\mathbf{1})^T$ is composed of the N_y-dimensional null vector $\mathbf{0}$ and $\mathbf{1} = (1, 0, ..., 0)$. The solution of the scattering Eq. **S34** determines the outgoing amplitude $A_{\mathrm{out}}^{(0)}$ by Eq. **24** in the main text.

Similar to the case for the linear network, when the driving frequency ω_{d} is resonant with the eigenfrequency $\mathcal{E}$ of the closed system, $a_{d,1}$ and the phase shift δ_0 are determined by Eqs. **25** and **26** in the main text. In the main text, we consider linear and nonlinear open networks in the cylindrical geometry. In the linear case, we study the detection of the energy spectrum through the phase shift δ_0. In the nonlinear case, we numerically solve Eq. **S34** for the network with size 24×12 and show the light distributions for different k_x and ω_{d} in Fig. 7 *C* and *D* of the main text.

For the open network in the plane shown in Fig. 2 *B* and *D* of the main text, the scattering equation for the amplitude $\mathbf{a} = (a_{r,nm}, a_{u,nm}, a_{l,nm}, a_{d,nm})^T$ reads

$$\bar{R}_{\mathrm{BM}} S_0\mathbf{a} = e^{-i\omega_{\mathrm{d}}L} e^{i\chi\mathcal{N}L}\mathbf{a} - t_{\mathrm{BM}} e^{-i\omega_{\mathrm{d}}L/2}\mathbf{A}_{\mathrm{in}}^{(0)}, \qquad \textbf{[S35]}$$

where $\bar{R}_{\mathrm{BM}}$ is obtained by replacing the diagonal matrix elements $I_{1,1}$ and $I_{3N_xN_y,3N_xN_y}$ of the $4N_xN_y$-dimensional identity matrix I by ir_{BM}, and $\mathbf{A}_{\mathrm{in}}^{(0)} = A_{\mathrm{in}}^{(0)}(\mathbf{1};\mathbf{0};\mathbf{0};\mathbf{0})^T$ is composed of the N_xN_y-dimensional null vector $\mathbf{0}$ and $\mathbf{1} = (1, 0, ..., 0)$. The solution of the scattering Eq. **S35** determines the reflection and transmission amplitudes by Eq. **28** in the main text.

In the main text, we study the light transmission to the linear network in the open plane. The solution of Eq. **S35** with $\chi = 0$ determines the light distribution in the linear network and the transmission probability $\left|A_{\mathrm{T}}/A_{\mathrm{in}}^{(0)}\right|^2$, which are shown in Fig. 4*B* of the main text for different driving frequency ω_{d}.

Robustness of Broadband Setups. In this section, we investigate the robustness of broadband models. To tune the topological bandwidth, we construct a new network, where the construction of the fiber is the same as that in Fig. 1*C* of the main text. As shown in Fig. S3, the node is built by four mirrors and one beam splitter in the center, where two birefringent elements (E, F) described by the Jones matrix σ_z in close proximity to the mirrors are connected to the horizontal fibers.

By the same procedure introduced in *Nodes* in the main text, we obtain the S-matrix $S_{\mathrm{node}} = S_1^{-1}S_2$ for each node, where

$$\begin{aligned} S_1 &= \frac{1}{t_{\mathrm{M}}}[I_4 + \sigma_x \otimes (r_{\mathrm{M}} r_{\mathrm{bs}}\sigma_x - ir_{\mathrm{M}} t_{\mathrm{bs}} I_2)], \\ S_2 &= \frac{1}{t_{\mathrm{M}}}(t_{\mathrm{bs}} I_4 + ir_{\mathrm{bs}} I_2 \otimes \sigma_x + ir_{\mathrm{M}}\sigma_x \otimes I_2) \end{aligned} \qquad \textbf{[S36]}$$

are determined by the 4×4 (2×2) matrix I_4 (I_2) and the reflection and transmission coefficients r_{M} (r_{bs}) and t_{M} (t_{bs}) of the mirrors (beam splitter).

The scattering equation at the bulk node in the linear network is

$$S_0\begin{pmatrix}a_{r,nm}\\a_{u,nm}\\a_{l,nm}\\a_{d,nm}\end{pmatrix}=e^{-i\omega L}\begin{pmatrix}a_{r,nm+1}\\a_{u,n-1m}\\a_{l,nm-1}\\a_{d,n+1m}\end{pmatrix},\qquad\textbf{[S37]}$$

where

$$S_0=\begin{pmatrix}e^{-in\sigma\theta_0}&0&0&0\\0&1&0&0\\0&0&e^{in\sigma\theta_0}&0\\0&0&0&1\end{pmatrix}S_{\rm node}.\qquad\textbf{[S38]}$$

We focus on the σ_+-polarized light with $\sigma=1$. With the different boundary conditions **11–13** in the main text, we can study the energy spectrum in the closed networks in the torus, cylinder, and open plane. We show the energy spectra in the cylindrical networks with different reflectivities $R_{\rm M}=|r_{\rm M}|^2=\{0.5,0.95,0.98\}$ in Fig. S4 *A–C*, where the chiral edge modes appear in the bandgaps. When $R_{\rm M}$ is increasing, the topological bandwidth becomes narrow.

The steady-state configuration of edge modes in the open linear network can be obtained by Eq. **S35**, where the pump field drives the network through the node $(1,1)$, and the node and each birefringent element have 0.1% intrinsic loss. As shown in Fig. S4 *D–F*, for the network with the same intrinsic loss, the steady edge state completely circulates around the boundary in the broadband setup with $R_{\rm M}=0.5$; however, the steady edge states can travel only a half or a quarter of the boundary in the narrow-band setup with $R_{\rm M}=0.95$ or 0.98, where $I=\sum_{s=r,u,l,d}|a_{s,nm}|^2$ is the light intensity at the node (n,m), and I_p is the intensity of the pump field.

Propagation Matrices of Bogoliubov Excitations. In this section, we define the propagation matrices of Bogoliubov excitations in *Bogoliubov Excitations in Nonlinear Optics* in the main text. The propagation matrices $\bar{P}_H=e^{\Sigma(\omega_{\rm f}-\bar{\mathbf{M}}_H)L}$ and $\bar{P}_V=e^{\Sigma(\omega_{\rm f}-\bar{\mathbf{M}}_V)L}$ for the Bogoliubov excitations in the horizontal and vertical fibers are determined by the matrices

$$\bar{\mathbf{M}}_H=\frac{\chi}{N_x}\begin{pmatrix}|a_{r,n}|^2&2e^{i(k_x-p_x)}\tilde{a}^*_{l,n}a_{r,n}&a^2_{r,n}&2e^{i(k_x-p_x)}a_{r,n}\tilde{a}_{l,n}\\2e^{-i(k_x-p_x)}a^*_{r,n}\tilde{a}_{l,n}&|\tilde{a}_{l,n}|^2&2e^{-i(k_x-p_x)}a_{r,n}\tilde{a}_{l,n}&\tilde{a}^2_{l,n}\\-a^{*2}_{r,n}&-2e^{i(k_x-p_x)}a^*_{r,n}\tilde{a}^*_{l,n}&-|a_{r,n}|^2&-2e^{i(k_x-p_x)}a^*_{r,n}\tilde{a}_{l,n}\\-2e^{-i(k_x-p_x)}a^*_{r,n}\tilde{a}^*_{l,n}&-\tilde{a}^{*2}_{l,n}&-2e^{-i(k_x-p_x)}\tilde{a}^*_{l,n}a_{r,n}&-|\tilde{a}_{l,n}|^2\end{pmatrix},\qquad\textbf{[S39]}$$

and

$$\bar{\mathbf{M}}_V=\frac{\chi}{N_x}\begin{pmatrix}|a_{u,n}|^2&2a^*_{d,n+1}a_{u,n}&a^2_{u,n}&2a_{u,n}a_{d,n+1}\\2a^*_{u,n}a_{d,n+1}&|a_{d,n+1}|^2&2a_{u,n}a_{d,n+1}&a^2_{d,n+1}\\-a^{*2}_{u,n}&-2a^*_{u,n}a^*_{d,n+1}&-|a_{u,n}|^2&-2a^*_{u,n}a_{d,n+1}\\-2a^*_{u,n}a^*_{d,n+1}&-a^{*2}_{d,n+1}&-2a^*_{d,n+1}a_{u,n}&-|a_{d,n+1}|^2\end{pmatrix},\qquad\textbf{[S40]}$$

where $\tilde{a}_{l,n}=e^{-in\sigma\theta_0}a_{l,n}$.

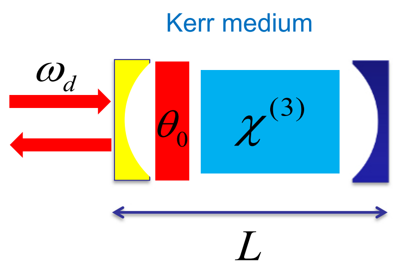

Fig. S1. A single Fabry–Perot cavity with Kerr nonlinearity and an anisotropic phase plate placed next to the left end mirror to mimic the horizontal link, where the driving field with frequency ω_d is applied.

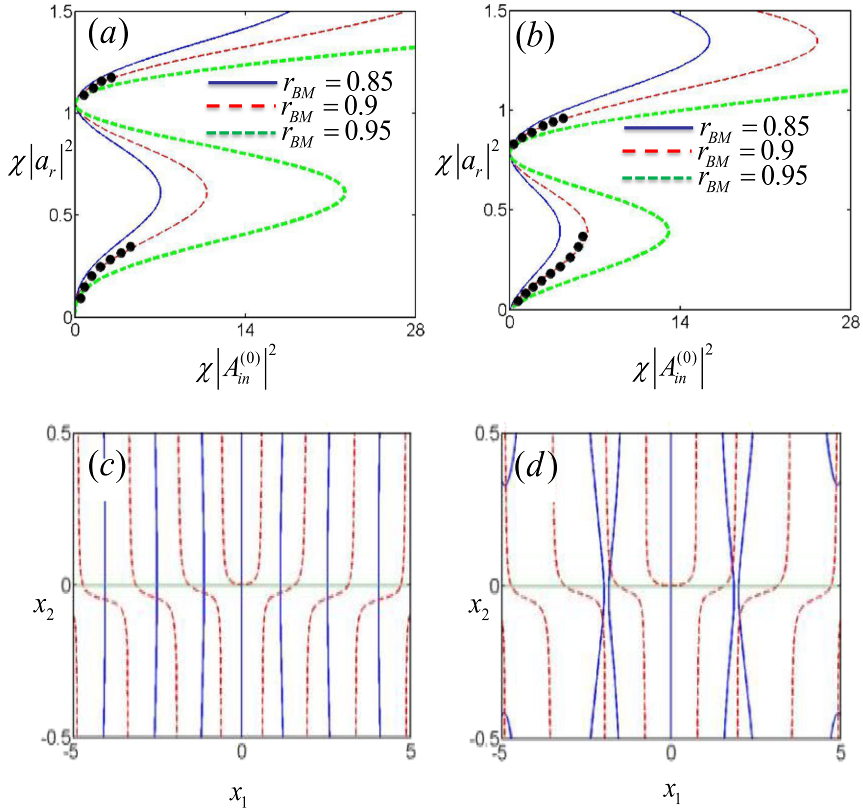

Fig. S2. Steady-state solutions and stability analysis, where L is taken as a unit. (*A* and *B*) The relation of the light intensity $\chi|a_r|^2$ in the cavity and the driving field intensity $\chi\left|A_{\mathrm{in}}^{(0)}\right|^2$ in steady state for the driving frequencies $\omega_d = 3\pi/4$ (*A*) and $\omega_d = \pi/2$ (*B*). Here, the stable regimes are marked by the black circles. The solid (blue), dashed (red), and dashed-dotted (green) curves denote the light intensities for $r_{\mathrm{BM}} = 0.85$, 0.9, and 0.95, respectively. (*C* and *D*) For $\omega_d = 3\pi/4$, the first and second equations in Eq. **27** are shown by the solid (blue) and dashed (red) curves, where $\chi|A_{\mathrm{in}}|^2 = 1$, $\chi|a_r|^2 = 1.12$ (*C*) and $\chi|A_{\mathrm{in}}|^2 = 5$, $\chi|a_r|^2 = 1.21$ (*D*).

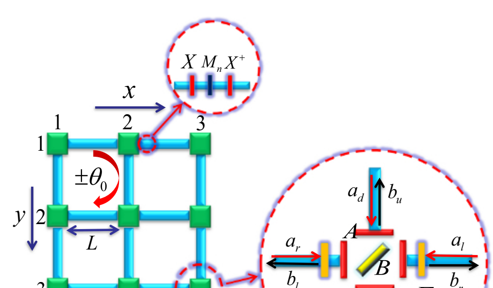

Fig. S3. The new setup with tunable topological bandgaps. Here, the fiber is constructed similar to that in Fig. 1*C* of the main text, but now each node is built by four transmissive mirrors *A* with reflection amplitude r_{M} and one beam-splitter *B* with reflection amplitude r_{bs}. Two birefringent elements (*E*, *F*) in close proximity to the mirrors are described by the Jones matrix σ_z.

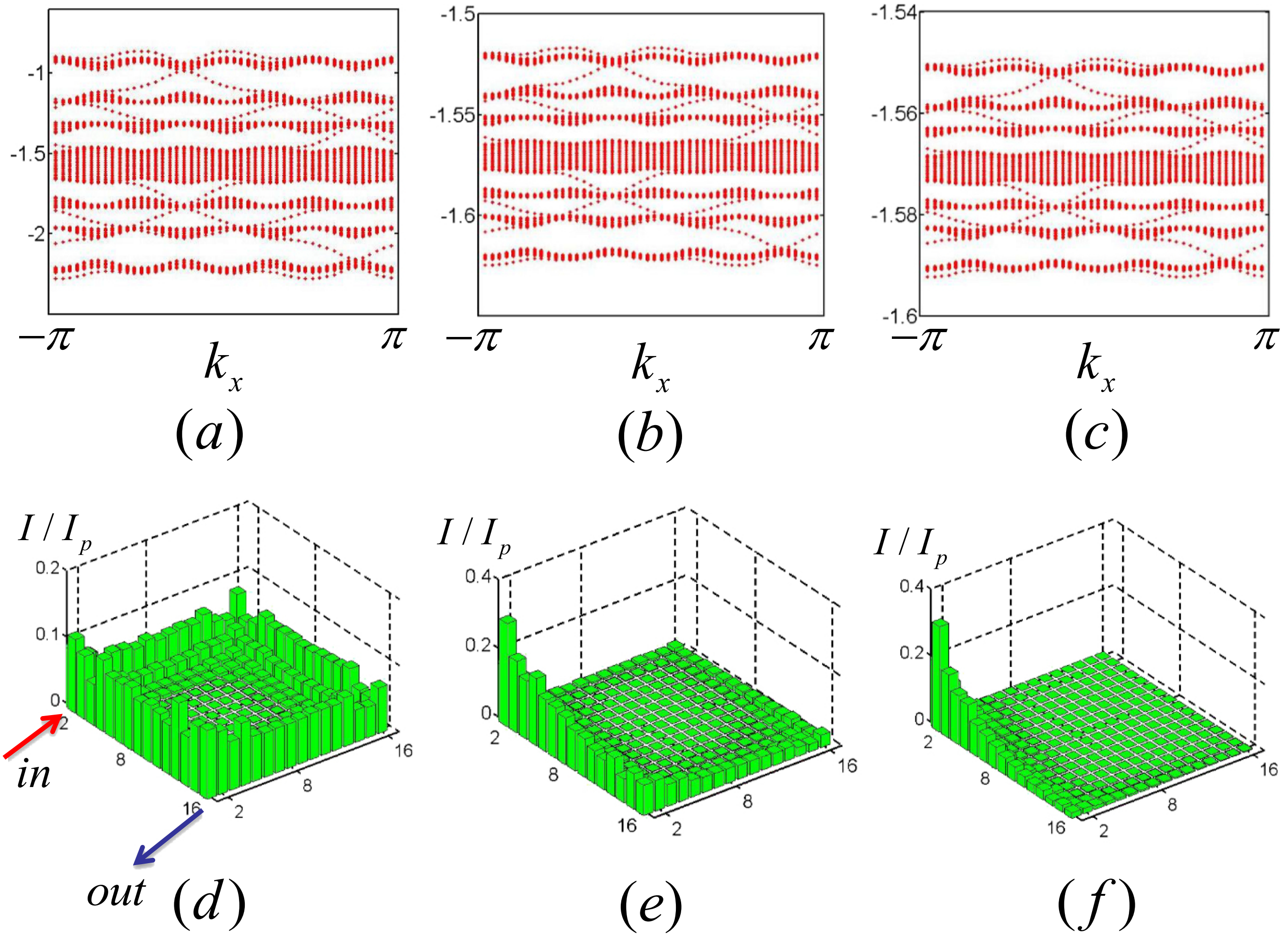

Fig. S4. (*A–C*) The energy spectra of the cylindrical network with 48 × 48 nodes for $R_m = |r_M|^2 = \{0.5, 0.95, 0.98\}$. (*D–F*) The light intensities of the steady edge modes in the open planar network with 16 × 16 nodes for $R_m = |r_M|^2 = \{0.5, 0.95, 0.98\}$, where the node and each birefringent element have 0.1% intrinsic loss.